IJE TRANSACTIONS A: Basics Vol. 37, No. 10, (October 2024) 1926-1935

International Journal of Engineering

Journal Homepage: www.ije.ir

Efficient Charging of Aerosol Nanoparticles by Corona-needle Charger with Improved Design for Printing of Metallic Microstructures

A. Efimov*, A. Patarashvili, D. Kornyushin, M. Ivanov, A. Lizunova, M. R. Ghorbani Fard, M. Nouraldeen, D. Labutov, V. Davydov, D. Maslennikov, M. Zebreva, V. Ivanov

Moscow Institute of Physics and Technology, National Research University, Dolgoprudny, Russia

P A P E R I N F O

Paper history:
Received 22 November 2023
Received in revised form 01 February 2024
Accepted 15 February 2024

Keywords:
Metallic Nanoparticles
Corona Discharge
Additive Manufacturing
Aerosol Charging
Electrostatic Precipitator
Microstructure

A B S T R A C T

Aerosol particle charging is widely used in various technical applications. A model of a needle-plate type charger for efficient charging of aerosol nanoparticles in a corona plasma discharge has been developed and investigated. The main difference from similar devices in the modernization of the grounded plate hole's geometry and the number of corona needles exist. This has resulted in a substantial increase in the charger's efficiency by over 25%. The effects of two types of discharge plates, one with cylindrical and the other with conical inner holes, on the extrinsic charging efficiency of aerosol particles were experimentally investigated. Metallic nanoparticles of Ag with sizes ranging from 20 to 160 nm and a number concentration of 10^6 to 10^8 cm^{-3} were utilized as the test aerosol. This system shows that the maximum efficiency of particle charging is attained by using a plate with a conical hole, which reduces electrostatic losses from 37±3% to 20±2%. Furthermore, an additional effect of increasing the particle charging efficiency was also observed by using a multi-pointed needle, which resulted in lower electrostatic losses compared to a single needle. Experimental evidence confirms that utilizing a conical hole in the plate and a multi-pointed needle has increased the particle charging efficiency from 47±3% to 59±4%, as opposed to the standard design featuring a cylindrical hole and a single-pointed needle. In this paper, an increase in the efficiency of charging particles in a charger with a multi-pointed needle compared to a single-pointed one is shown for the first time.

doi: *10.5829/ije.2024.37.10a.06*

Graphical Abstract

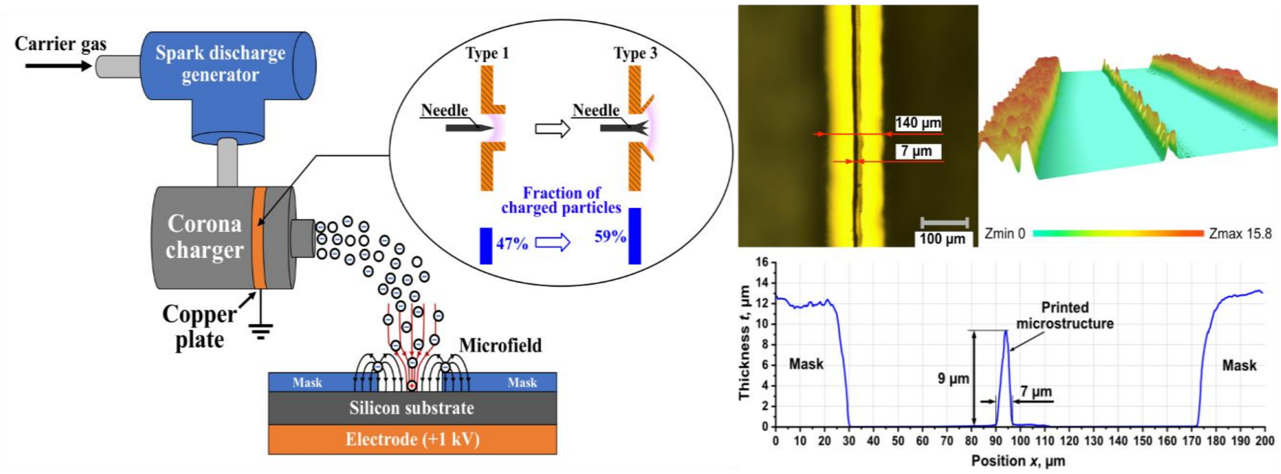

*Corresponding Author Email: efimov.aa@mipt.ru (A. Efimov)

Please cite this article as: Efimov A, Patarashvili A, Kornyushin D, Ivanov M, Lizunova A, Ghorbani Fard MR, Nouraldeen M, Labutov D, Davydov V, Maslennikov D, Zebreva M, Ivanov V. Efficient Charging of Aerosol Nanoparticles by Corona-needle Charger with Improved Design for Printing of Metallic Microstructures. International Journal of Engineering, Transactions A: Basics. 2024;37(10):1926-35.

NOMENCLATURE

L_E	Electrostatic losses of particles (%)	d_1	Smaller diameter of the conical hole in the plate (mm)
N_i	Ion concentration (cm^{-3})	d_2	Larger diameter of the conical hole in the plate (mm)
Q_{sh}	Sheath flow (lpm)	l	Conical hole depth (mm)
Q_a	Aerosol flow (lpm)	n	Number of points in multi-pointed copper needle
Z_i	Electrical mobility of ions (m^2/(V·s))	r	Tungsten needle radius of curvature (μm)
E	Electric field strength (V/m)	R	Copper needle radius of curvature (μm)
n_1	Particle concentration at the outlet with NPC and ESP turned off (cm^{-3})	**Greek Symbols**	
n_2	Particle concentration at the outlet with NPC on and ESP off (cm^{-3})	η_{extr}	Extrinsic particle charging efficiency (%)
n_3	Particle concentration at the outlet with NPC and ESP turned on (cm^{-3})	η_{intr}	Intrinsic particle charging efficiency (%)
A	Effective anode surface area (m^2)	β	The field enhancement coefficient
e	Elementary electric charge (C)	**Abbreviations**	
I	Corona discharge current (μA)	NPC	Nanoparticle charger
U	Corona discharge voltage (kV)	ESP	Electrostatic precipitator
d_p	Particle size (nm)	DC	Direct current
h	The fraction of uncharged particles (%)	SDG	Spark discharge generator
d	Diameter of cylindrical hole in plate (mm)	AR	Aspect ratio

1.INTRODUCTION

Nanoparticles with electrical charge are increasingly being used in practical applications. Their ability to be controlled using electric or magnetic fields is particularly interesting, as it enables a wide range of potential uses. Furthermore, in this paper also presents a distinctive investigation into the design of electrodes, suggesting that existing chargers could be greatly enhanced through simple modifications. Effective charging of aerosols is essential for achieving high concentrations and reducing material costs in 3D printing, and can be achieved through methods like corona discharge charging, as well as optimization of particle size and concentration (1, 2). Improving aerosol charging efficiency is especially important for printing metallized micro- and nanostructures, where reducing coagulation is essential (3). Aerosol charging is also used in differential electrical mobility measurements (4, 5). By increasing the charging efficiency of nanoparticles, material consumption and costs can be reduced in additive manufacturing (6-9). On the other hand, to achieve high-speed printing of micro- or nanostructures, a significant amount of nanoparticles is required as building blocks (10). Functional nanoparticles are widely used both in the form of an aerosol (11, 12) and in a colloidal solution (nanofluid) (13). However, increasing the concentration of particles also leads to higher losses due to Coulomb mutual repulsion (14). Therefore, developing chargers that can efficiently work with highly concentrated aerosols is challenging. This article investigates the diffusion mechanism involved in the charging (15, 16) of Ag nanoparticles with sizes ranging from 20 to 160 nm and at a high concentration of 10^6-10^8 cm^{-3} (17). To charge particles, a needle-plate charger is utilized to create a unipolar ion cloud through DC corona discharge, resulting in the movement of ions towards the particle surface to transfer charge. Various wire and needle corona ionizer designs for particle charging have been detailed in published works (14, 16, 18-20). To evaluate the effectiveness of an ionizer, the charging efficiency is a critical factor. It refers to the percentage of charged particles among all particles that reach the ionizer input. A desirable ionizer should have a high η_{extr} value for extrinsic charging efficiency, indicating that a high proportion of particles are charged. Additionally, a high N_i value for ion concentration is preferred, indicating that a large number of ions are generated. Finally, a low L_E value for electrostatic losses of particles is desirable, indicating that fewer particles are lost due to electrostatic forces. Overall, an ideal ionizer should have high η_{extr} and N_i values and a low L_E value. The charger described in this article can charge nanoparticles with the highest efficiency η_{extr}=59±4% with sizes between 20 and 160 nm. While, it has a simple and compact design, it provides low diffusion, inertial and electrostatic losses. Improving the charger's efficiency has multiple benefits, including reducing material consumption, especially when using costly materials like in printing. Additionally, it lowers the speed of device contamination. This enables you to achieve a charger that operates more consistently and for a longer period of time without needing to be cleaned. In this work, experiments were carried out using polydisperse metallic nanoparticles of Ag obtained by spark discharge between silver electrodes (21-27). It is known that this synthesis method provides a high number concentration (10^6–10^8 cm^{-3}) aerosol nanoparticles that quickly coagulate, resulting in a broadening of the particle size distribution.

The charging process of a highly concentrated aerosol is further complicated by the mutual repulsion of charged particles, resulting in electrostatic losses L_E. For this purpose, in this regard, in this work the known geometry of the Nanoparticle charger (NPC) was modified for working with polydisperse aerosol. Specifically, changes were made to the design of the plate and the needle, with addition of sheath flow Q_{sh} to guarantee a high extrinsic particle charging efficiency η_{extr} across various particle sizes. Furthermore, the modified NPC was employed to create nanoparticle microstructures on a silicon substrate through the technique of aerosol lithography aided by an electric field, to showcase its operational benefits and efficacy.

2. MATERIALS AND METHODS

To enhance comprehension, Figure 1 illustrates the sketch of the updated Nanoparticle charger, which allows for interchangeable needles and plates. A needle is inserted into a polyamide dielectric body under the potential of a high voltage supplied from a source IVNR-30/1 (Plazon, Russia). The sharp part of the needle is located in a hole in a grounded copper plate so that the space between the tip of the needle and the edge of the hole forms a volumetric of corona plasma region (see Figure 1). Aerosol nanoparticles passing through the plasma collide with ions and electrons and acquire electrical charges (15, 28-33). The Q_a aerosol flow was supplied through a 6 mm diameter hole in the top of the sheath. The absence of sharp corners in the path of aerosol movement allows one to avoid inertial losses of particles. Moreover, the body of NPC has a hole for supplying a sheath flow Q_{sh} in order to reduce electrostatic losses of particles on the walls of the plate. The ion concentration in the region of the volume corona charge N_i was determined by the Equation 1:

$$N_i = \frac{I}{Z_i \cdot E \cdot A \cdot e} \tag{1}$$

where I – corona discharge current
Z_i – electrical mobility of ions;
E – electric field strength;
A – effective anode surface area;
e – elementary electric charge.

The value of the corona discharge current I was measured using an M-42300 microammeter. To ensure effective functioning of the charger, the ion concentration N_i must be significantly higher (2-3 orders of magnitude) than the particle concentration (34). The ion concentration calculated in experiments was 10^{11}–10^{12} cm^{-3}, which satisfies these conditions. The aerosol flow rate Q_a with numerical concentration n_0 at the outlet of the spark discharge generator (SDG) was 1 lpm (Figure 2). This particle size distribution is characterized by a lognormal function (5, 35). The aerosol flow passes through the charging device and is then directed to the electrostatic precipitator (ESP). When activated, this precipitator traps all electrically charged particle in the flow (Figure 2).

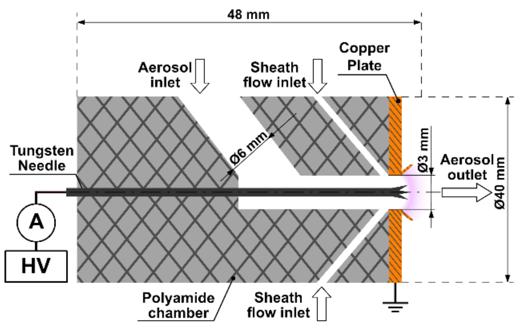

Figure 1. Sketch of the developed Nanoparticle charger with replaceable corona needles and copper plates.

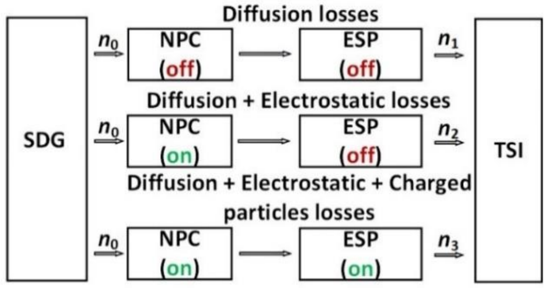

Figure 2. Experimental design to measure charger performance.

Finally, an aerosol spectrometer (SMPS 3936, TSI Inc., Shoreview, MN, USA) was connected to the ESP outlet to allow real-time measurement of particle size and concentration in the aerosol flow.

In these experiments, a well-known method was used to evaluate the charger efficiency, taking into account the geometry of the discharge electrodes (needle and plate) and the value of the sheath flow (Q_{sh}) (14, 15). This method required conducting consecutive measurements of particle number concentrations with the NPC and ESP in both active (turned on) and inactive (turned off) states (as illustrated in Figure 2), with the objective of calculating the values for the intrinsic charging efficiency η_{intr}, electrostatic losses L_E, and the fraction of uncharged particles h, using the following equations:

$$\eta_{intr} = \frac{n_1 - n_2}{n_1} \tag{2}$$

$$L_E = \frac{n_1 - n_2}{n_1} \tag{3}$$

$$h = \frac{n_3}{n_2} \tag{4}$$

where n_1 – particulate matter concentration at the outlet when both the NPC and ESP are inactive (turned off);
n_2 – particle concentration at the outlet with the NPC active (turned on) and the ESP inactive (turned off);
n_3 – particle concentration at the outlet when both the NPC and ESP are active (turned on);

The extrinsic particle charging efficiency η_{extr}, which is the main performance parameter of the charger, is determined by the following equation:

$$\eta_{extr} = \frac{n_2 - n_3}{n_1} \tag{5}$$

Parameters η_{intr}, L_E, h, and η_{extr} are commonly used in practice and are selected as main characteristics to evaluate NPC performance (14). For example, the intrinsic charging efficiency η_{intr} represents the fraction of initially neutral particles that acquire a charge while inside the charger, regardless of whether they leave the charger or not. Electrostatic particle losses L_E refer to the fraction of charged particles that are lost in the charger due to electrostatic forces. The extrinsic charging efficiency, η_{extr}, is the most important parameter for practical use, and it is determined by the ratio of the concentration of charged particles at the outlet of the system (n_2-n_3) to the initial concentration of particles (n_1) entering the charger.

Experiments were conducted to evaluate the efficiency of the charger for plates and needles of various geometries, as previous studies indicated that charged particles are significantly lost on them (14, 36, 37). In the experiments, particle charging was studied for three types of discharge electrode geometries (needles and plates) at different values of the sheath flow rate Q_{sh}. A schematic representation of these types is presented in Figure 3. The first and second types (Figures 3a and 3b) of discharge electrodes were a single-point needle located inside a cylindrical and conical hole of the plate, respectively, and the third type (Figure 3c) was a multi-point needle inside a conical hole. The diameter of the cylindrical hole in the plate is d=3mm with a depth of L=4mm, and the conical hole has diameters of d_1=3mm, d_2=8mm, and a depth of l=2mm. Both the single-pointed tungsten needle and the multi-pointed copper needle (8 points) have radii of curvature equal to r=32 and R=42 µm, respectively.

It is a well-established fact that, for long-term needle use, it is advisable to use materials that resist ion bombardment and the adsorption and desorption of residual gas molecules. Typically, the materials used for manufacture corona needles include refractory metals (such as W, Re, Pt, Mo) and transition group metals (including Cr, Nb, Hf). Nonetheless, there are some challenges involved in the machining of refractory materials.

In this work, a combination of a single-point refractory needle and a multi-pointed copper needle was utilized. The use of a copper needle is suitable for short-term work, as the softness of this metal significantly eases the process of creating multi-point tips.

To demonstrate the applicability of the developed charger, it was used in aerosol lithography with an electric field, to create metal microstructures from nanoparticles that are pertinent to electronic and optical uses.

3. RESULTS

The results of measurements of parameter values η_{intr}, L_E, h, and η_{extr}, for different types of discharge electrodes (Type 1–3) and various sheath flow rates Q_{sh}= (1–3) lpm, are shown in Figure 4. The experiments were performed at a constant corona discharge current of I=20 µA, with the corona discharge voltage U being adjusted. The results depicted in Figure 4 indicate that in all cases, an increase in the values of Q_{sh} leads to a reduction in electrostatic losses L_E and an increase in the proportion of uncharged particles h. It is known that further increase Q_{sh} would lead to too much dilution of the concentration of nanoparticles, which is a negative effect (14).

For the purpose of convenience of analysis, Table 1 presents the values η_{intr}, L_E and η_{extr}=(η_{intr}–L_E), received from Q_{sh}=3 lpm for the case of a single-point and multi-point needle and a cylindrical and conical hole in the plate, respectively. In the case of using a single-point needle and a plate with a cylindrical hole (Type 1), the maximum value of the extrinsic charging efficiency η_{extr} is 47±3% at Q_{sh}=3 lpm, as shown in Table 1. The shape of the plate hole was altered to a truncated cone in order to minimize the electrostatic losses L_E on the plate (Type 2). From a comparison of Figures 4 (a and

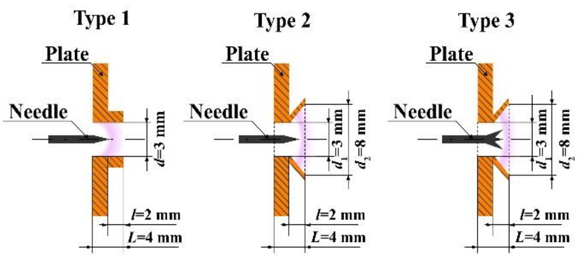

(a) (b) (c)

Figure 3. The schematic represents the corona charge region with a single-point tungsten needle inside a plate with a (a) cylindrical and (b) conical hole, as well as a multi-point copper needle inside a plate with a (c) conical hole

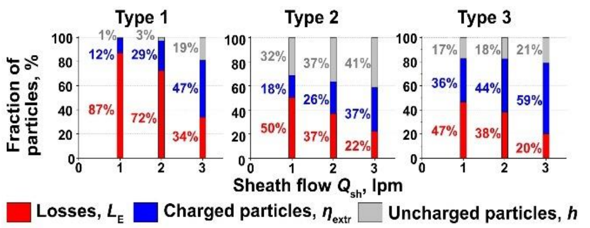

(a) (b) (c)

Figure 4. Dependence of charger characteristics (L_E, h and η_{extr}) when using three types of discharge electrodes (Type 1–3) for different values of sheath flows Q_{sh} equal to 1, 2 and 3 lpm. which consist of (a) Type 1 and Q_{sh}=1-3, (b) Type 2 and Q_{sh}=1-3, (c) Type 3 and Q_{sh}=1-3.

b) it can be seen that the electrostatic losses L_E have indeed decreased.

Nevertheless, altering the geometry of the hole in the plate also resulted in a significant increase in the proportion of uncharged particles *h* due to the reduced ion concentration N_i in the corona plasma, as shown in equation 1, because at a constant current *I*, it was necessary to increase the corona voltage *U* from -2.4 to -2.7 kV, as shown in Table 1. The decision was made to increase the number of points on the needle to 8 in order to counteract this effect (Type 3), as shown in Figure 4(c). This change did indeed lead to a notable reduction in the proportion of uncharged particles *h* while keeping the electrostatic losses L_E unchanged.

Figure 5 illustrates the processes taking place inside the charger. The particles move along the main axis of the needle, after which they fall into the corona discharge region. Particles acquire an electric charge with a certain probability, which depends on the concentration of ions and the time the particle is in a given area. Charged particles are exposed to a strong electric field that attracts them to the plate. Approaching the walls of the plate, the flow of enveloping gas prevents their deposition. Thus, a decrease in electrostatic losses of particles from 34% (type 1) to 22% (type 2) when changing the shape of the hole in the plate is due to the complication of their movement towards the plate walls (see Table 1). When changing the shape of the needle, a higher ion concentration is obtained, which accompanies an increase in intrinsic charging efficiency from 59% (type 2) to 79% (type 3). As a result, an increase in extrinsic charging efficiency of particles from 47% (type 1) to 59% (type 2) obtained.

In comparison to recent studies by Hrasa et al. (38) and Saputra et al. (39), this research demonstrates that the charger has higher intrinsic and extrinsic charging efficiency. This is because bipolar devices are less efficient for charging due to the recombination of ion charges. However, in the aforementioned studies, chargers have very low losses, which reduces the risk of device contamination and the need for cleaning. Therefore, the choice of device depends on the set goals.

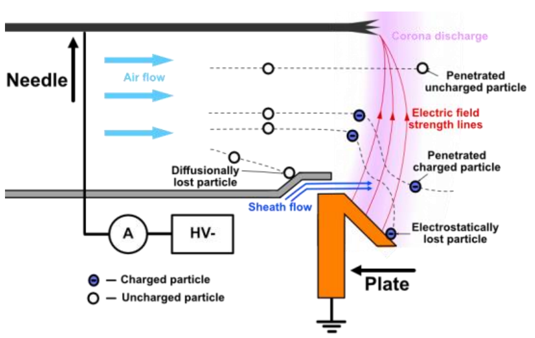

Figure 5. Illustration of the particle charging and losses processes occurring within the aerosol charger

TABLE 1. Charger parameters when assessing its operating efficiency at Q_{sh}=3 lpm.

Name of discharge electrodes	*I*, μA	*U*, kV	Intrinsic efficiency η_{intr}	Electrostatic losses L_E	Extrinsic efficiency η_{extr}
Type 1	20	−2.4	81%	34%	47%
Type 2	20	−2.7	59%	22%	37%
Type 3	20	−2.1	79%	20%	59%

When a cylindrical hole and a single-pointed needle are used (Figures 2a and 4a), the electric field lines are nearly perpendicular to the direction of particle flow. This design is commonly used in many devices of this type. On the other hand, when utilizing a plate with a truncated cone-shaped hole (Figures 2b and 4b), charged particles must counter the aerosol and sheath flows to be deposited on the plate, leading to reduced electrostatic losses (L_E). However, the discharge voltage in this scenario is higher at -2.7 kV instead of -2.4 kV. Consequently, the intrinsic charging efficiency (η_{intr}) decreases due to a reduction in ion concentration, as outlined in equation 1. On the contrary, when using a multi-point needle and a conical hole (Figures 2c and 4c), the ion concentration can be increased by reducing the discharge voltage *U* at the same current value *I*, as shown in Table 1. Thus, it ensures high intrinsic charging efficiency η_{intr}, and low losses are achieved by the fact that charged particles also have to go against the aerosol and sheath flows. The photographs of the single-point tungsten and multi-point copper needles used in the experiments are displayed in Figure 6.

Preliminary studies have indicated that the proportion of diffusion-deposited particles is less than 5–10% of the initial concentration (14, 40, 41) and is independent of the shape of the electrodes. Therefore, in further experiments, diffusion losses were not considered when calculating the charging efficiency. Electrostatic losses L_E arise when an electric field acts on charged particles. This effect is particularly pronounced in the corona plasma region, and excessive voltage or an extended charging area can result in increased losses. The sheath

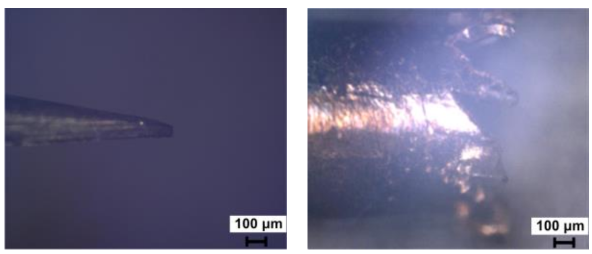

(a) (b)

Figure 6. Photographs of (a) a single-point tungsten needle and (b) a multi-point copper needle measured using a Keyence VHX-1000 optical microscope

flow Q_{sh} interferes with this process and removes charged particles, preventing them from reaching the plate.

It is known that one of the main parameters determining the emission properties of tip cathodes is the field enhancement coefficient β (see equation 6). This coefficient is equal to the ratio of the maximum electric field strength E_{max} to its average value $\bar{E} = U/d$, where U – the voltage across the needle, and d is the distance between the needle and the plate.

$$\beta = \frac{E_{max}}{\bar{E}} \tag{6}$$

The maximum field enhancement factor β_{max} of a single tip is primarily determined, as a first approximation, by its aspect ratio (the value of the ratio $H/2R_0$), where H represents the tip height and R_0 denotes the radius of its curvature. When the tip height is fixed, the coefficient β_{max} increases as the radius of curvature decreases and, for a constant radius, it increases with the height of the tips. As β_{max} grows, the current-voltage characteristics shift towards the region of lower voltages. To minimize the shielding of adjacent points, it is advised to select a distance between points (L) that is equal to or greater than twice the height of the needle (H) ($L \geq 2H$) in the case of a multi-point needle. The study found that for an eight-pointed needle with a radius (R) of 42 µm, an average distance (L) of 400 µm and height (H) of 200 µm was optimal. The tungsten needle had a radius of curvature of 32 µm.

To achieve better results, the field enhancement factor β was increased by ensuring a small radius of curvature of the tips (R=42 µm) and the required length of each tip (H=200 µm). Additionally, increasing the number of tips from 1 to 8 at a given distance between them (L=400 µm) allowed for a high concentration of ions N_i with minimal electrical potential on the needle.

Furthermore, the intrinsic and extrinsic efficiency of particle charging, denoted as η_{intr} and η_{extr}, were investigated based on their size d_p for geometries Type 1–3 (Figures 6 and 7) at different flow rates Q_{sh}. Figure 8 illustrates the dependence of extrinsic particle charging efficiency η_{extr} on their size d_p for different sheath flows Q_{sh}.

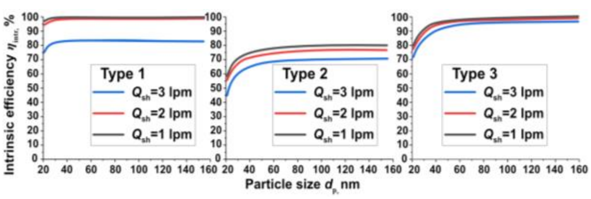

(a) (b) (c)

Figure 7. Dependence of intrinsic particle charging efficiency η_{intr} on their size d_p for different sheath flows Q_{sh} with (a) Type 1, (b) Type 2 and (c) Type 3

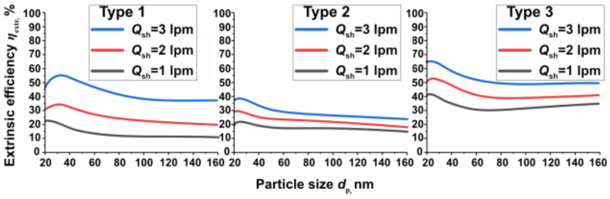

(a) (b) (c)

Figure 8. Dependence of extrinsic particle charging efficiency η_{extr} on their size d_p for different sheath flows Q_{sh} with (a) Type 1, (b) Type 2 and (c) Type 3

The highest extrinsic particle charging efficiency, η_{extr}, is achieved for particles ranging in size from 20 to 60 nm. However, it is important to consider that charging also reduces the coagulation of particles and increases the number of small particles at the output by decreasing the concentration of large particles.

Figures 6 and 7 show that the improved needle and plate geometry of the designed charger results in higher extrinsic particle charging efficiencies, η_{extr}. This is due to the reduction of electrostatic losses, L_E, through changes in the shape of the plate, while maintaining high intrinsic charging efficiency values, η_{intr}, by replacing a needle with a multi-pointed one.

The particle charging process is known to play a key role in the printing of functional micro- and nanostructures (42). To demonstrate the applicability of the developed charger in the technology of printing micro- and nanostructures, the deposition of charged metallic nanoparticles of Ag on a silicon substrate through a dielectric mask made of polyvinyl chloride (PVC) was performed (10). Figure 9 illustrates the experimental design for printing metal microstructures by utilizing a developed charger and a dielectric mask.

A flow of aerosol silver particles, ranging in size from 20 to 160 nm, was generated in a spark discharge generator and then directed to the charger. Subsequently,

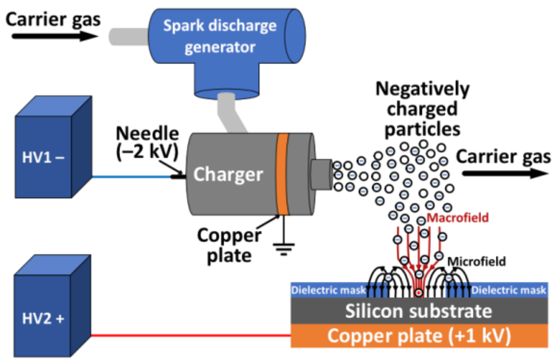

Figure 9. Schematic diagram of an experiment to print silver nanoparticle microstructures on a silicon substrate by depositing charged nanoparticles through a dielectric PVC mask using a fabricated corona charger

the negatively charged aerosol nanoparticles that emerged from the charger were transported by a carrier gas along a PVC dielectric mask to deposit onto the surface of the silicon substrate through an opening in the mask. The dielectric mask had a thickness of 13 µm, and the gap was 140 µm width and several millimeters length. Furthermore, a 0.5 mm thick silicon substrate was fixed to a copper plate under a positive potential of +1 kV to attract particles with opposite charges (see Figure 9). It is important to mention that the printed microstructures were much narrower than the gaps in the mask. Figure 10 displays a picture and a profile of a silver nanoparticle microstructure created by depositing them through a dielectric mask for an hour. The optical microscope (VHX-1000, Keyence, Osaka, Japan) and 3D profilometer (S neox, Sensofar, Terrassa, Spain) were used to measure the image and profile of the microstructure and mask, respectively.

According to Figure 10, the microstructures of Ag nanoparticles that were deposited form a line with a width of 7±1 µm. This width is more than 20 times smaller than the gap in the mask. This result is attributed to the creation of an electric microfield on the surface of the dielectric mask, which is caused by the deposition of charged particles and anions. As a result, electric field strength lines are formed from the mask, which are directed towards the center of the silicon substrate (43, 44). This phenomenon is further explained in studies conducted by Martins et al. (45) and Rusinque et al. (46). It is worth noting that the printed line has a high aspect ratio (AR=thickness/width) of 1.3, which is a typical compared to lines produced through traditional printing methods such as aerosol jet (2), inkjet (47), or direct writing (48).

Obviously, the fabrication of micro- and nanostructures requires a constant supply of building blocks in the form of charged aerosol nanoparticles. In this work, a corona charger was used to create such building blocks, which has demonstrated its effectiveness. It is known that such technologies allow the production of micro- and nanostructures from nanoparticles that are used in chemical (49) and gas (50) sensors, electronics products (51), optics (52) and energy conversion systems (53). Thus, the developed charger has great potential for further development of contactless printing technologies.

After studying the basic recommendations for operating the device, a scheme was proposed to achieve high charging efficiency of the device (as shown in Figure 11).

It is also possible to consider the integration of artificial intelligence into this charger, which will be able to analyze the degree of contamination of the device and needle wear by the level of voltage and current of the corona discharge (54).

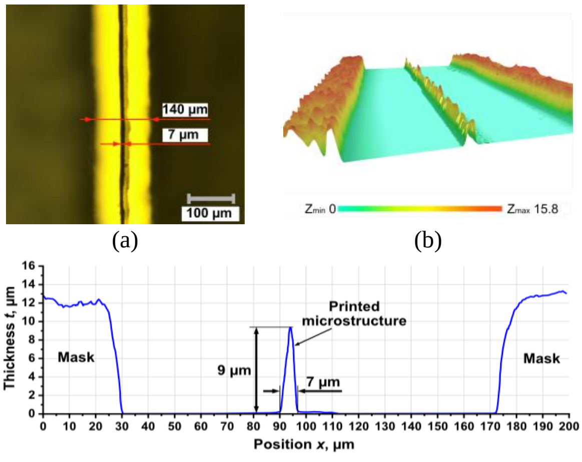

Figure 10. Optical image (a), 3D (b) and 2D (c) cross-sectional profile of a microstructure of Ag nanoparticles formed on a silicon substrate by electrostatic deposition of charged aerosol through a PVC dielectric mask

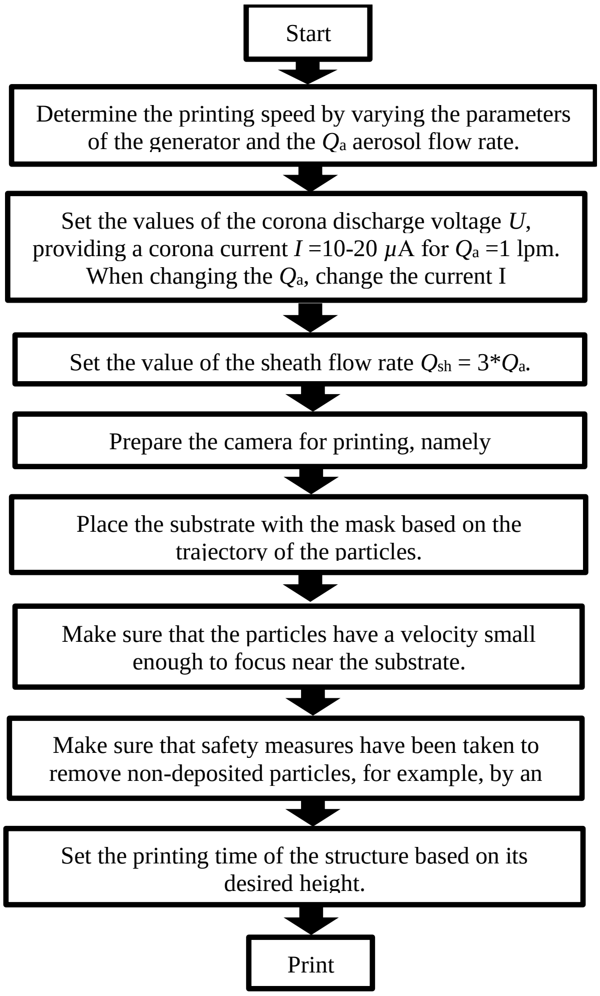

Figure 11. A flowchart for selecting optimal parameters for efficient particle charging

4. CONCLUSIONS

The article describes the development and testing of a modified needle-plate charger for unipolar charging of metallic aerosol nanoparticles. The charger uses a needle at a high electric potential and a grounded plate with a hole to create a volumetric corona discharge that charges the nanoparticles. In addition, different shapes and positions of the electrodes were tested, and it was observed that changing the geometry can improve the extrinsic charging efficiency from 47% to 59% and reduce electrostatic losses during charging from 34% to 20% for high nanoparticle concentrations. The modified charger was also used to create metallic microstructures through electrostatic deposition of nanoparticles on a silicon substrate using a dielectric mask. Overall, the article highlights the potential of this technology for improving material usage efficiency and extending the duration of continuous usage with high-speed printing.

5. ACKNOWLEDGMENTS

This research was funded by the Russian Science Foundation grant No. 22-79-10127, https://rscf.ru/project/22-79-10127/, as part of studies of unipolar charging of aerosol nanoparticles, grant No. 22-19-00311, https://rscf.ru/project/22-19-00311/, as part of the investigation into the size and elemental composition of nanoparticles and the Ministry of Science and Higher Education of the Russian Federation (stated contract No. 075-03-2023-106, project identifier FSMG-2022-0036) as part of optimization synthesis of nanoparticles by spark discharge generator.

6. REFERENCES

1. Park J, Jeong J, Kim C, Hwang J. Deposition of Charged Aerosol Particles on a Substrate by Collimating Through an Electric Field Assisted Coaxial Flow Nozzle. Aerosol Science and Technology. 2013;47. 10.1080/02786826.2013.767981
2. Jung W, Jung Y-H, Pikhitsa PV, Feng J, Yang Y, Kim M, et al. Three-dimensional nanoprinting via charged aerosol jets. Nature. 2021;592(7852):54-9. 10.1038/s41586-021-03353-1
3. Park K-T, Massoudi Farid M, Hwang J. Anti-agglomeration of spark discharge-generated aerosols via unipolar air ions. Journal of Aerosol Science. 2013;67. 10.1016/j.jaerosci.2013.09.009
4. Wang SC, Flagan RC. Scanning electrical mobility spectrometer. Journal of Aerosol Science. 1989;20(8):1485-8. 10.1016/0021-8502(89)90868-9
5. Efimov A, Ivanov V, Volkov IA, Subbotina I, Pershin N. Filtration of nanosized particle aerosols by electret fibrous filters. Nanotechnologies in Russia. 2013; 8. 10.1134/S1995078013060062
6. Liu B, Liu S, Devaraj V, Yin Y, Zhang Y, Ai J, et al. Metal 3D nanoprinting with coupled fields. Nature Communications. 2023;14(1):4920. 10.1038/s41467-023-40577-3
7. Khecho A, Ghaffari SA, Behzadnasab M, Rahmat M. Role of Mixing Method and Solid Content on Printability of Alumina Inks for Stereolithography 3D Printing Process. International Journal of Engineering, Transactions C: Aspects. 2022;35(3):580-6. 10.5829/ije.2022.35.03C.11
8. Oladapo BI, Balogun V. Electrical Energy Demand Modeling of 3D Printing Technology for Sustainable Manufacture. International Journal of Engineering, Transactions A: Basics. 2016;29(7):954-61. doi: 10.5829/idosi.ije.2016.29.07a.10
9. Sri Harsha A, Vikram Kumar CR. Fused Deposition Modeling of an Aircraft Wing using Industrial Robot with Non-linear Tool Path Generation. International Journal of Engineering, Transactions A: Basics. 2021;34(1):272-82. 10.5829/ije.2021.34.01a.30
10. Spark Ablation: Building Blocks for Nanotechnology. New York: Jenny Stanford Publishing; 2020 2020-02-07. 472 p.
11. Gautam M, Kim JO, Yong CS. Fabrication of aerosol-based nanoparticles and their applications in biomedical fields. Journal of Pharmaceutical Investigation. 2021;51(4):361-75. 10.1007/s40005-021-00523-1
12. Muldarisnur M, Perdana I, Elvaswer E, Puryanti D. Mapping of Sensing Performance of Concentric and Non-Concentric Silver Nanoring. Emerging Science Journal. 2023;7(4):1083-99. 10.28991/ESJ-2023-07-04-04
13. Arifin Z, Khairunisa N, Kristiawan B, Prasetyo SD, Bangun WB. Performance Analysis of Nanofluid-based Photovoltaic Thermal Collector with Different Convection Cooling Flow. Civil Engineering Journal. 2023;9(8):1922-35. 10.28991/CEJ-2023-09-08-08
14. Alonso M, Martin MI, Alguacil FJ. The measurement of charging efficiencies and losses of aerosol nanoparticles in a corona charger. Journal of Electrostatics. 2006;64(3):203-14. 10.1016/j.elstat.2005.05.008
15. Zheng C, Chang Q, Lu Q, Yang Z, Gao X, Cen K. Developments in Unipolar Charging of Airborne Particles: Theories, Simulations and Measurements. Aerosol and Air Quality Research. 2016;16(12):3037-54. 10.4209/aaqr.2016.07.0319
16. Alisoy HZ, Alagoz S, Alisoy GH, Alagoz BB. A numerical method for the analysis of polydisperse aerosol particles charging in a coaxial electrode system. Journal of Electrostatics. 2012;70(1):111-6. 10.1016/j.elstat.2011.11.004
17. Intra P, Tippayawong N. Design and Evaluation of a High Concentration, High Penetration Unipolar Corona Ionizer for Electrostatic Discharge and Aerosol Charging. Journal of Electrical Engineering and Technology. 2013;8(5):1175-81. 10.5370/JEET.2013.8.5.1175
18. Medved A, Dorman F, Kaufman SL, Pöcher A. A new corona-based charger for aerosol particles. Journal of Aerosol Science. 2000;31:616-7. 10.1016/S0021-8502(00)90625-6
19. Intra P, Yawootti A. An Experimental Investigation of A Non-Mixing Type Corona-Needle Charger for Submicron Aerosol Particles. Journal of Electrical Engineering & Technology. 2019;14(1):363-70. 10.1007/s42835-018-00011-x
20. Qi C, Chen D-R, Greenberg P. Performance study of a unipolar aerosol mini-charger for a personal nanoparticle sizer. Journal of Aerosol Science. 2008;39(5):450-9. 10.1016/j.jaerosci.2008.01.003
21. Tabrizi NS, Ullmann M, Vons VA, Lafont U, Schmidt-Ott A. Generation of nanoparticles by spark discharge. Journal of Nanoparticle Research. 2009;11(2):315-32. 10.1007/s11051-008-9407-y
22. Kornyushin D, Musaev A, Patarashvili A, Buchnev A, Arsenov P, Ivanov M, et al. Effect of the Gas Temperature on Agglomeration of Au Nanoparticles Synthesized by Spark Discharge and Their Application in Surface-Enhanced Raman Spectroscopy. Metals. 2023;13(2):301. 10.3390/met13020301

23. Efimov AA, Arsenov PV, Borisov VI, Buchnev AI, Lizunova AA, Kornyushin DV, et al. Synthesis of Nanoparticles by Spark Discharge as a Facile and Versatile Technique of Preparing Highly Conductive Pt Nano-Ink for Printed Electronics. Nanomaterials. 2021;11(1):234. 10.3390/nano11010234

24. van Ginkel HJ, Mitterhuber L, van de Putte MW, Huijben M, Vollebregt S, Zhang G. Nanostructured Thermoelectric Films Synthesised by Spark Ablation and Their Oxidation Behaviour. Nanomaterials. 2023;13(11):1778. 10.3390/nano13111778

25. Němec T, Šonský J, Gruber J, de Prado E, Kupčík J, Klementová M. Platinum and platinum oxide nanoparticles generated by unipolar spark discharge. Journal of Aerosol Science. 2020;141:105502. 10.1016/j.jaerosci.2019.105502

26. Efimov AA, Kornyushin DV, Buchnev AI, Kameneva EI, Lizunova AA, Arsenov PV, et al. Fabrication of Conductive and Gas-Sensing Microstructures Using Focused Deposition of Copper Nanoparticles Synthesized by Spark Discharge. Applied Sciences. 2021;11(13):5791. 10.3390/app11135791

27. Zhang J, Ahmadi M, Fargas G, Perinka N, Reguera J, Lanceros-Méndez S, et al. Silver Nanoparticles for Conductive Inks: From Synthesis and Ink Formulation to Their Use in Printing Technologies. Metals. 2022;12(2):234. 10.3390/met12020234

28. Chen J, Davidson J. Ozone Production in the Negative DC Corona: The Dependence of Discharge Polarity. Plasma Chemistry and Plasma Processing. 2003;23:501-18. 10.1023/A:1023235032455

29. Yawootti A, Intra P, Tippayawong N, Rattanadecho P. An experimental study of relative humidity and air flow effects on positive and negative corona discharges in a corona-needle charger. Journal of Electrostatics. 2015;77:116-22. 10.1016/j.elstat.2015.07.011

30. Quakernaat J. Handbook of electrostatic processes: J.S. Chang, A.J. Kelly, J.M. Crowley (Eds) Marcel Dekker, New York, 1995, 763pp, ISBN 8247-9254-8, $195.00. Journal of Cleaner Production. 1995;3(3):175. 10.1016/0959-6526(95)90001-2

31. Marquard A, Kasper M, Meyer J, Kasper G. Nanoparticle charging efficiencies and related charging conditions in a wire-tube ESP at DC energization. Journal of Electrostatics. 2005;63(6):693-8. 10.1016/j.elstat.2005.03.032

32. Hinds WC. Aerosol Technology: Properties, Behavior, and Measurement of Airborne Particles: John Wiley & Sons; 2012 2012-12-06. 482 p.

33. Alisoy HZ, Alagoz BB, Alisoy GH. An analysis of corona field charging kinetics for polydisperse aerosol particles by considering concentration and mobility. Journal of Physics D: Applied Physics. 2010;43(36):365205. 10.1088/0022-3727/43/36/365205

34. Adachi M, Kousaka Y, Okuyama K. Unipolar and Bipolar Diffusion Charging of Ultrafine Aerosol Particles. Journal of Aerosol Science. 1985;15:109-23. 10.1016/0021-8502(85)90079-5

35. Park D, Kim Y-H, Lee S-G, Kim C, Hwang J, Kim Y-J. Development and performance test of a micromachined unipolar charger for measurements of submicron aerosol particles having a log-normal size distribution. Journal of Aerosol Science. 2010;41(5):490-500. 10.1016/j.jaerosci.2010.02.007

36. Intra P, Wanusbodeepaisarn P, Siri-achawawath T. Evaluation of the Performance in Charging Efficiencies and Losses of Ultrafine Particles Ranging in Sizes from 15 to 75 nm in a Unipolar Corona-based Ionizer. Journal of Electrical Engineering & Technology. 2021;16(2):963-74. 10.1007/s42835-020-00623-2

37. Intra P, Tippayawong N. Use of electrostatic precipitation for excess ion trapping in an electrical aerosol detector. Journal of Electrostatics. 2011;69(4):320-7. 10.1016/j.elstat.2011.04.008

38. Krasa H, Schriefl MA, Kupper M, Melischnig A, Bergmann A. Aerosol Charging with a Piezoelectric Plasma Generator. Plasma. 2021;4(3):377-88. 10.3390/plasma4030027

39. Saputra C, Kamil AI, Munir MM, Waris A, Novitrian. The performance of an electrical ionizer as a bipolar aerosol charger for charging ultrafine particles. Aerosol Science and Technology. 2022;56(2):117-33. 10.1080/02786826.2021.1976719

40. Huang C-H, Lin Y-C, Chang C-L. Penetration Efficiency and Concentration Distribution of Nanoparticles in a Hollow Tapered Cylinder. Applied Sciences. 2022;12(16):8025. 10.3390/app12168025

41. Huang C-H, Cheng Y-H. Numerical Investigation of Ultrafine Aerosol Deposition inside a Needle Charger without Applied Voltage. Atmosphere. 2022;13(5):695. 10.3390/atmos13050695

42. Jung W, Pikhitsa PV, Jung Y-H, Shin J, Han M, Choi M. 3D Nanoprinting with Charged Aerosol Particles─An Overview. Accounts of Materials Research. 2021;2(11):1117-28. 10.1021/accountsmr.1c00187

43. Choi H, Kang S, Jung W, Jung Y-h, Park SJ, Kim DS, et al. Controlled electrostatic focusing of charged aerosol nanoparticles via an electrified mask. Journal of Aerosol Science. 2015;88:90-7. 10.1016/j.jaerosci.2015.05.017

44. Krinke TJ, Fissan H, Deppert K. Deposition of Aerosol Nanoparticles on Flat Substrate Surfaces. Phase Transitions. 2003;76(4-5):333-45. 10.1080/0141590210000514 51

45. Martins V, Cruz Minguillón M, Moreno T, Querol X, de Miguel E, Capdevila M, et al. Deposition of aerosol particles from a subway microenvironment in the human respiratory tract. Journal of Aerosol Science. 2015;90:103-13. 10.1016/j.jaerosci.2015.08.008

46. Rusinque H, Fedianina E, Weber A, Brenner G. Numerical study of the controlled electrodeposition of charged nanoparticles in an electric field. Journal of Aerosol Science. 2019;129:28-39. 10.1016/j.jaerosci.2018.11.005

47. Sim I, Park S, Shin K-Y, Yang C, Kang H, Hwang JY, et al. Inkjet Printing of High Aspect Ratio Silver Lines via Laser-Induced Selective Surface Wetting Technique. Coatings. 2023;13(4):683. 10.3390/coatings13040683

48. Wu S, Zhang J, Wang Z, Chen Y, Huang G, Liu Y, et al. High-aspect-ratio silver grids of solar cells prepared by direct writing. Solar Energy Materials and Solar Cells. 2023; 259: 112452. 10.1016/j.solmat.2023.112452

49. Jung K, Hahn J, In S, Bae Y, Lee H, Pikhitsa PV, et al. Hotspot-Engineered 3D Multipetal Flower Assemblies for Surface-Enhanced Raman Spectroscopy. Advanced Materials. 2014;26(34):5924-9. 10.1002/adma.201401004

50. Bae Y, Pikhitsa PV, Cho H, Choi M. Multifurcation Assembly of Charged Aerosols and Its Application to 3D Structured Gas Sensors. Advanced Materials. 2017;29(2):1604159. 10.1002/adma.201604159

51. Lewis JA, Ahn BY. Three-dimensional printed electronics. Nature. 2015;518(7537):42-3. 10.1038/518042a

52. Gansel JK, Thiel M, Rill MS, Decker M, Bade K, Saile V, et al. Gold Helix Photonic Metamaterial as Broadband Circular Polarizer. Science. 2009;325(5947):1513-5. 10.1126/science.1177031

53. Li J, Liang X, Liou F, Park J. Macro-/Micro-Controlled 3D Lithium-Ion Batteries via Additive Manufacturing and Electric Field Processing. Scientific Reports. 2018;8(1):1846. 10.1038/s41598-018-20329-w

54. Widjaja RG, Asrol M, Agustono I, Djuana E, Harito C, Elwirehardja GN, et al. State of Charge Estimation of Lead Acid Battery using Neural Network for Advanced Renewable Energy Systems. Emerging Science Journal. 2023;7(3):691-703. 10.28991/ESJ-2023-07-03-02

Persian Abstract

چکیده

شارژ ذرات آئروسل به طور گسترده در کاربردهای فنی مختلف استفاده می شود. مدلی از یک شارژر صفحه سوزنی برای شارژ کارآمد نانوذرات آئروسل در تخلیه پلاسمای کرونا توسعه و بررسی شده است. تفاوت اصلی آن با دستگاه های مشابه در مدرن سازی هندسه سوراخ صفحه زمین و تعداد سوزن های تاج است. این امر منجر به افزایش قابل توجهی در راندمان شارژر تا بیش از ۲۵ درصد شده است. اثرات دو نوع صفحه تخلیه، یکی با سوراخ‌های استوانه‌ای و دیگری با سوراخ‌های داخلی مخروطی، بر راندمان شارژ بیرونی ذرات آئروسل به طور تجربی مورد بررسی قرار گرفت. نانوذرات فلزی نقره با اندازه‌های ۲۰ تا ۱۶۰ نانومتر و غلظت cm^{-3} ۱۰۶– ۱۰۸ به عنوان آئروسل آزمایشی مورد استفاده قرار گرفتند. این سیستم نشان می دهد که حداکثر بازده شارژ ذرات با استفاده از صفحه ای با سوراخ مخروطی شکل حاصل می شود، که تلفات الکترواستاتیکی را از ۳±۳۷ درصد به ۲±۲۰ درصد کاهش می دهد. علاوه بر این، یک اثر اضافی افزایش بازده شارژ ذرات نیز با استفاده از یک سوزن چند نقطه مشاهده شد که منجر به تلفات الکترواستاتیک کمتری نسبت به یک سوزن منفرد شد. شواهد تجربی تأیید می‌کنند که استفاده از یک سوراخ مخروطی در صفحه و یک سوزن چند نقطه، بازده شارژ ذرات را از ۳±۴۷ درصد به ٤±۵۹ درصد افزایش داده که برخلاف طرح استانداردی است که دارای یک سوراخ استوانه‌ای و یک سوزن تک نوک است. در این مقاله برای اولین بار افزایش راندمان شارژ ذرات در یک شارژر با سوزن چند نقطه نسبت به یک سوزن تک نقطه نشان داده شده است.